

# Realization of a 5-Bit NMR Quantum Computer Using a New Molecular Architecture

R. Marx

*Institut für Organische Chemie, J. W. Goethe-Universität, Marie-Curie-Str. 11,  
D-60439 Frankfurt, Germany*

A. F. Fahmy

*Biological Chemistry and Molecular Pharmacology, Harvard Medical School,  
240 Longwood Avenue, Boston, MA 02115, USA*

John M. Myers

*Gordon McKay Laboratory, Division of Engineering and Applied Sciences,  
Harvard University, Cambridge, MA 02138, USA*

W. Bermel

*Bruker Analytik GmbH, Silberstreifen, D-76287 Rheinstetten, Germany*

S. J. Glaser

*Institut für Organische Chemie und Biochemie, Technische Universität München,  
Lichtenbergstr. 4, D-85748 Garching, Germany*

We demonstrate a five-bit nuclear-magnetic-resonance quantum computer that distinguishes among various functions on four bits, making use of quantum parallelism. Its construction draws on the recognition of the sufficiency of linear coupling along a chain of nuclear spins, the synthesis of a suitably coupled molecule, and the use of a multi-channel spectrometer.

## I. INTRODUCTION

While quantum computers of two bits have been implemented [1], as have nuclear-magnetic-resonance (NMR) quantum computers of three bits [2], extending the number of bits has not proved easy. We report the implementation of an NMR quantum computer having five bits, involving the use of a linear coupling pattern [3], synthesis of a molecule having five usable spin-active nuclei with predominantly linear spin-spin coupling, and the development of radio-frequency (r.f.) pulse sequences to act as quantum logic gates for the molecule synthesized. Techniques to suppress unwanted couplings between nuclear spins are described, as are techniques to avoid perturbing some nuclear spins while manipulating others. Results are presented of a test of the five-bit computer on a problem of Deutsch and Jozsa to distinguish one class of mathematical function from another [4].

## II. DEFINITION OF AN $n$ -BIT NMR COMPUTER

An  $n$ -bit quantum computer is called on to do three things: 1) accept an instruction to prepare a starting

state and prepare that state; 2) accept instructions for and implement quantum gates (from which more general unitary transformations of the state can be composed); and 3) measure the state and yield an outcome. The connection to computation with classical computers depends on the recognition, due to Bennett [5], that all classical computations can be made reversible. Any terminating reversible computation is a permutation of the inputs, which is unitary, and thus belongs to the class of transformation performable on a quantum computer. (For issues of possibly nonterminating programs, see [6].)

In theory, a variant of the quantum computer is the expectation-value quantum computer (EVQC), which in place of an outcome of a measurement yields the expectation value [7,8]. NMR quantum computing was born of the recognition that an EVQC can be approximated by use of an NMR spectrometer containing a liquid sample, the molecules of which have  $n$  atoms with a nuclear spin of  $1/2$  (and possibly other atoms, either spinless or having spins not used) [7,8,9]. Because tumbling of the molecules decouples each molecule from all the others, the sample can be

described by a density matrix for the nuclear spins of the atoms of a single molecule [10], with only the spin-degrees of freedom, corresponding to the desired Hilbert space of dimension  $2^n$ . NMR spectrometers sense only the traceless part of the density matrix, so in place of matter in a pure state, an NMR computer can use a liquid sample described by a density matrix proportional to a sum of a pure state and any multiple of the unit matrix. Such a density matrix, called a *pseudopure* state [7], plays a role in the 5-bit quantum computer.

Acting as an  $n$ -bit EVQC, a suitable NMR spectrome-

ter allows the preparation of a pseudopure starting state, the programming and execution of r.f. pulse sequences that implement quantum gates, and the

determination of expectation values visible in NMR spectra. To perform the unitary operations required of a quantum computer, a sufficient set of quantum gates consists of all single-spin operations and all controlled-not gates that act on one nuclear spin under the control of another nuclear spin. Single-spin gates are implemented by selective r.f. pulses. Controlled-not gates between nuclei having spin-spin coupling will be described, along with techniques to avoid unwanted influences on other spins. A key feature of the present design of the NMR quantum computer is the reliance on a chain of linear coupling and the use of swap gates to implement a controlled-not in which a spin  $j$  controls spin  $k$ , where  $j$  and  $k$  have no direct spin-spin coupling [3]. This allows use in NMR quantum computers of a molecule having a simpler coupling pattern, and eases the problem of unwanted influences on spins.

### III. DESIGN OF TEST

The proof of the pudding is in the eating: the 5-bit NMR computer to be described was tested on the Deutsch-Jozsa problem for functions of 4 bits [4], in the form described in [11], modified for efficiency with NMR as described by Jones and Mosca [12]. (A recent simplification [13], unused here, would permit working with functions of 5 bits.) The problem is to decide whether a function program selected from a set of possible programs computes one kind of function or another. Specifically, the problem is to distinguish programs for balanced functions from programs for constant functions, where the functions are from  $\{0, 1\}^4$  to  $\{0, 1\}$ . (A function is constant if its value is independent of its argument, and is called balanced if the value for half the arguments is 1 while the value is 0 for the other half.) The test actually made was to distinguish between programs for one constant and one balanced function, defined as follows:

$$f_0(\vec{x}) \stackrel{\text{def}}{=} 0 \quad (1)$$

and

$$f_b(\vec{x}) \stackrel{\text{def}}{=} x_1 \oplus x_2 \oplus x_3 \oplus x_4 \quad (2)$$

for all  $\vec{x}$ , where  $\vec{x} \stackrel{\text{def}}{=} (x_1, x_2, x_3, x_4)$ , and “ $\oplus$ ” is addition modulo 2. Also, several controlled-not (CNOT) gates were tested, along with a variety of 1-bit operators. The balanced function chosen,  $f_b$ , has the nice property of being implementable also in classical reversible gates with no work bits.

Used to solve this problem, a quantum computer is a resource used both to specify the function under test

and to determine what it is. In order to separate these two uses, one can view the quantum computer as used alternately by a *specifier* of the function and a *decision maker*, two players of a game in which: (A) the decision maker prepares the starting state; (B) the specifier runs the function program;<sup>1</sup> and (C) the decision maker makes a measurement independent of the function program, and interprets the result to decide the function class.

On an NMR quantum computer, (A) the decision maker starts a play by using r.f. pulses and magnetic-field gradients (independent of the function to be specified) to put the liquid sample in the pseudopure state having a density matrix with a traceless part proportional to

$$\rho_i \stackrel{\text{def}}{=} 16|00001\rangle\langle 00001| - \frac{1}{2}\mathbf{1} = 16I_1^\alpha I_2^\alpha I_3^\alpha I_4^\alpha I_5^\beta - \frac{1}{2}\mathbf{1} \quad (3)$$

in terms of the polarization operators  $I_k^\alpha = (\frac{1}{2}\mathbf{1} + I_{kz})$  and  $I_k^\beta = (\frac{1}{2}\mathbf{1} - I_{kz})$  usual to NMR [10,3]. Then the decision maker applies a unitary transform  $U_{90}$  by use of a hard  $90^\circ$   $y$ -pulse which for this particular state has the same effect as the Hadamard transform on each spin [12].

$$\begin{aligned} \rho_i \xrightarrow{U_{90}} \rho_0 &= U_{90}\rho_i U_{90}^\dagger \\ &= 16 \left(\frac{1}{2}\mathbf{1} + I_{1x}\right) \left(\frac{1}{2}\mathbf{1} + I_{2x}\right) \left(\frac{1}{2}\mathbf{1} + I_{3x}\right) \\ &\quad \times \left(\frac{1}{2}\mathbf{1} + I_{4x}\right) \left(\frac{1}{2}\mathbf{1} - I_{5x}\right) - \frac{1}{2}\mathbf{1}. \end{aligned} \quad (4)$$

(B) The specifier chooses a function  $f$  from one of the set of functions undergoing test, here  $f_0$  or  $f_b$ , and runs the quantum version of a program to compute  $f$ ; this program is a sequence of gates, each a unitary transformation implemented by an r.f. pulse sequence. The total program implements a unitary transformation  $U(f)$ ,

defined by its action on basis vectors  $|\vec{x}, x_5\rangle$ :

$$U(f)|\vec{x}, x_5\rangle = |\vec{x}, x_5 \oplus f(\vec{x})\rangle. \quad (5)$$

The transform  $U(f)$  produces the density matrix with traceless part proportional to  $\rho_f$ :

$$\rho_0 \xrightarrow{U(f)} \rho_f. \quad (6)$$

(C) The decision maker reads out the NMR spectrum which depends on  $\rho_f$ . The spectrum differs according to whether  $f$  is balanced or constant, and thus tells the decision maker the function class, with only one function evaluation, a large saving over classical computation, which could require 9 evaluations for functions of four bits.

---

<sup>1</sup>These two moves must be iterated for a classical computer, but not in the quantum solution of the Deutsch-Jozsa problem, giving the quantum computer a large advantage over the classical computer.

In theory, for the case  $f = f_0$ ,  $U(f)$  is specified to be  $U(f_0)$ , which by Eqs. (1) and (5) turns out to be the identity matrix, so one should have  $\rho_f = \rho_0$ . The spectrometer detects only the terms of the righthand side of Eq. (4) that are linear in  $I_x$ , so for a spectrometer adjusted to give an upward peak for  $I_x$ , the resulting spectrum is in theory  $\underline{\text{||||}}$ , which has, from left to right, positive peaks for spins 1 to 4 and a negative peak for spin 5.

For the balanced function,  $f = f_b$  (Eq. (2)),  $U(f_b)$  is defined by  $U(f_b)|\vec{x}, x_5\rangle = |\vec{x}, x_1 \oplus x_2 \oplus x_3 \oplus x_4 \oplus x_5\rangle$ . A unitary operator that is simpler to implement, that has the same effect on the fifth (value) bit, and that allows the distinction between constant and balanced functions is  $\tilde{U}(f_b)$  defined by

$$\tilde{U}(f_b)|\vec{x}, x_5\rangle = |x_1, x_1 \oplus x_2, x_1 \oplus x_2 \oplus x_3, x_1 \oplus x_2 \oplus x_3 \oplus x_4, x_1 \oplus x_2 \oplus x_3 \oplus x_4 \oplus x_5\rangle, \quad (7)$$

which we implemented by sequential application of the gates  $(\text{CNOT})_{12}$ ,  $(\text{CNOT})_{23}$ ,  $(\text{CNOT})_{34}$ , and  $(\text{CNOT})_{45}$ . The spectrum calculated for the density matrix  $\tilde{\rho}_b$  obtained by transforming  $\rho_0$  with  $\tilde{U}(f_b)$  is  $\underline{\text{||||}}$  (*vide infra*).

#### IV. REALIZATION AND TEST OF A 5-BIT NMR COMPUTER

A 5-bit NMR quantum computer requires a molecule having 5 spin-active nuclei, with long relaxation times. Large separation of resonance frequencies of the nuclei allows rapid selective control of the spins. For frequency separation, it is desirable to use different atomic species for different spins, which requires a multi-channel NMR spectrometer. Our NMR experiments were performed using a BRUKER AVANCE 400 spectrometer with five independent r.f. channels and a QXI probe (H,C-F,N). The lock coil was also used for deuterium decoupling utilizing a lock switch. A linear path of spin-spin couplings is sufficient for all computations [3]. Given the availability of a 5-channel spectrometer, we chose as the ‘‘hardware’’ of our NMR quantum computing experiments the molecule BOC-( $^{13}\text{C}_2$ - $^{15}\text{N}$ - $^2\text{D}_2^\alpha$ -glycine)-fluoride which contains an isolated coupling network consisting of five nuclei, each having spin 1/2: the amide  $^1\text{H}$ , the  $^{15}\text{N}$ , the aliphatic  $^{13}\text{C}^\alpha$ , the carbonyl  $^{13}\text{C}'$ , and the  $^{19}\text{F}$  nuclear spin (see Fig. 1). For simplicity, we will refer to these spins (and the corresponding bits) as 1, 2, 3, 4 and 5, respectively. All spins are heteronuclear, except for  $\text{C}^\alpha$  and  $\text{C}'$  which however have a relatively large chemical shift difference. The five-spin system is well isolated from the protons of the BOC protecting group which are separated by more than four chemical bonds. In addition, the deuterium spins (D) which are attached to  $\text{C}^\alpha$  can be fully decoupled from the spins of interest using standard heteronuclear decoupling techniques [14,15,16]. The

substance was synthesized starting from commercially available  $^{13}\text{C}$  and  $^{15}\text{N}$  labeled glycine (see Appendix A) and was dissolved in deuterated dimethylsulfoxide (DMSO- $\text{D}_6$ ). NMR experiments were performed at a magnetic field of about 9.4 Tesla and a sample temperature of 27° C. The experimentally determined  $T_2$  relaxation times for spins 1–5 were 250 ms, 490 ms, 450 ms, 590 ms, and 260 ms, respectively. Resonance frequencies  $\nu_k$  and scalar coupling constants  $J_{kl}$  are summarized in Table I. Except for the  $J_{23}$  coupling constant of 13.5 Hz, the spin chain is connected by one-bond coupling constants  $J_{k\{k+1\}}$  larger than 60 Hz. In the multiple rotating frame (see Ref. [10] and Appendix B) the precession frequency of each individual spin is 0, which considerably simplifies implementation, because only coupling terms need to be considered (and manipulated).

TABLE I. Resonance frequencies  $\nu_k$ , chemical shifts  $\delta_k$ , one-bond coupling constants  $J_{k\{k+1\}}$ , and non-zero two-bond coupling constants  $J_{k\{k+2\}}$  of the used five-spin system. No resolved three- or four-bond coupling constants were observed.

$\nu_1 = 400, 133, 001.6$ Hz	$(\delta_1 = 7.51$ ppm)
$\nu_2 = 40, 547, 895.3$ Hz	$(\delta_2 = 75.54$ ppm)
$\nu_3 = 100, 616, 858.0$ Hz	$(\delta_3 = 41.05$ ppm)
$\nu_4 = 100, 629, 089.1$ Hz	$(\delta_4 = 162.61$ ppm)
$\nu_5 = 376, 510, 545.5$ Hz	$(\delta_5 = 31.92$ ppm)
$J_{12} = 94.1$ Hz	$J_{23} = 13.5$ Hz
$J_{34} = 65.2$ Hz	$J_{45} = 366.0$ Hz
$J_{13} = 2.7$ Hz	$J_{35} = 67.7$ Hz

TABLE II. List of initial Cartesian product operator terms of  $\rho_i$  (Eqs. (3) and (8)) that give rise to detectable signals for at least one of the functions  $f_0$  or  $f_b$  in the implemented version [11] of the Deutsch-Jozsa algorithm (see also Appendices B and C). The propagators  $U(f_0) = \mathbf{1}$  and  $\tilde{U}(f_b)$  (Eq. (7)) transform  $\rho_0$  (Eq. (4)) to  $\rho_0$  and  $\tilde{\rho}_b$ , respectively (Eq. (6)). Only the underlined terms of  $\rho_0$  and  $\tilde{\rho}_b$  which contain single transverse spin operators correspond to single quantum coherences that are detectable in an NMR experiment.

$\rho_i$	$\rho_0$	$\tilde{\rho}_b$
$I_{1z}$	<u><math>I_{1x}</math></u>	$16I_{1x}I_{2x}I_{3x}I_{4x}I_{5x}$
$2I_{1z}I_{2z}$	$2I_{1x}I_{2x}$	<u><math>I_{1x}</math></u>
$I_{2z}$	<u><math>I_{2x}</math></u>	$8I_{2x}I_{3x}I_{4x}I_{5x}$
$2I_{2z}I_{3z}$	$2I_{2x}I_{3x}$	<u><math>I_{2x}</math></u>
$I_{3z}$	<u><math>I_{3x}</math></u>	$4I_{3x}I_{4x}I_{5x}$
$2I_{3z}I_{4z}$	$2I_{3x}I_{4x}$	<u><math>I_{3x}</math></u>
$I_{4z}$	<u><math>I_{4x}</math></u>	$2I_{4x}I_{5x}$
$-2I_{4z}I_{5z}$	$-2I_{4x}I_{5x}$	<u><math>-I_{4x}</math></u>
$-I_{5z}$	<u><math>-I_{5x}</math></u>	<u><math>-I_{5x}</math></u>

The experimental implementation of the propagator  $U(f_0)$  corresponding to  $f_0$  is trivial because by Eq. (5) the propagator is the unit operator, implemented by doing nothing. In contrast, the construction of the pulse sequence to implement the series of CNOT-gates that define the unitary transformation  $\tilde{U}(f_b)$  of Eq. (7) for the balanced function  $f_b$  (Eq. (2)) requires attention. The goal is to create robust pulse sequence elements that minimize the effects of experimental imperfections. The pulse sequence elements shown in Fig. 2 A-D were designed specifically for the coupling topology of our 5-spin system to implement the unitary operators corresponding to  $(\text{CNOT})_{12}$ ,  $(\text{CNOT})_{23}$ ,  $(\text{CNOT})_{34}$ , and  $(\text{CNOT})_{45}$ .<sup>2</sup> During these CNOT gates that act on two directly coupled spins  $k$  and  $l$ , only the couplings  $J_{kl}$  are active, while the effect of all other couplings in the spin system are refocused by cyclic pulse sequences [10,17,18]. Figure 3 shows schematically the pulse sequence actually used for the propagator  $\tilde{U}(f_b)$  for the balanced function  $f_b$ ; this sequence benefited from applying simple rules for pulse cancellation (see Appendix B.2).

The NMR implementation of the Deutsch-Jozsa algorithm starts with the preparation of the pseudopure state  $\rho_i$  of Eq. (3). The preparation of such a pseudopure state by a single pulse sequence requires a non-unitary transformation of the thermal equilibrium density operator [7,19]. This can be achieved using spatial averaging [7,3] or temporal averaging [7,20]. In the basis formed by Cartesian product operators [10],  $\rho_i$  can be expressed as a linear combination of 31 terms that only consist of  $z$  spin operators:

$$\begin{aligned} \rho_i = & \sum_{n=1}^5 s_n I_{nz} + \sum_{m<n} s_n 2I_{mz}I_{nz} + \sum_{l<m<n} s_n 4I_{lz}I_{mz}I_{nz} \\ & + \sum_{k<l<m<n} s_n 8I_{kz}I_{lz}I_{mz}I_{nz} - 16I_{1z}I_{2z}I_{3z}I_{4z}I_{5z}, \end{aligned} \quad (8)$$

where  $s_n = -1$  if  $n = 5$  and  $s_n = 1$  otherwise. It is straightforward to create each of these terms from the thermal equilibrium density operator, using standard building blocks of high-resolution NMR [21]. In principle, temporal averaging could be realized by repeating steps (A)–(C) of the game for all 31 terms in Eq. (8) and

---

<sup>2</sup>During each pulse sequence shown in Fig. 2 only the coupling  $J_{kl}$  is active which is required in order to implement  $(\text{CNOT})_{kl}$ . The effects of other non-zero couplings (see Table I) are effectively eliminated, except for  $J_{13}$  in the sequence implementing  $(\text{CNOT})_{45}$  (Fig. 2 D). Although it would be straightforward to remove also this coupling, this would require additional pulses which can be avoided because in our spin system the coupling  $J_{13} = 2.7$  has a negligible effect during the relatively short duration  $\Delta_{45} = 1/(2J_{45}) = 1.39$  ms of this gate.

by summing up the resulting spectra. However, because currently available NMR spectrometers require a distinct experiment to detect each spin species ( $^1\text{H}$ ,  $^{15}\text{N}$ ,  $^{13}\text{C}$  and  $^{19}\text{F}$ ) (see Appendix B.3), a total of 124 NMR experiments would be required for each function  $f$  in order to include all terms in the temporal averaging. A detailed analysis shows that of the 31 terms that constitute the pseudopure state  $\rho_i$ , only the five linear terms  $I_{kz}$  and the four bilinear terms  $2I_{kz}I_{\{k+1\}z}$  are transformed into detectable operators by the propagator  $U_{90}$  (to create  $\rho_0$ ) followed by the propagators  $U(f_0)$  or  $\tilde{U}(f_b)$ , as the case may be (see Table II and Appendix C). As pointed out previously [2], preparing just the

linear terms  $I_{kz}$  suffices in some cases of the Deutsch-Jozsa problem to distinguish constant from balanced functions, because in these cases a balanced function gives a vanishing signal for at least one of the input spins. However, in the presence of experimental imperfections, it is desirable to identify a balanced function based on the sign reversal of the signal of at least one of the input spins, rather than by the lack of a signal. For the special case of the balanced function  $f_b$  that was chosen for this demonstration experiment, this can be achieved by including also the bilinear terms  $2I_{kz}I_{\{k+1\}z}$  as starting operators (see Table II).

Samples described by these linear and bilinear terms of  $\rho_i$  were prepared (see Appendix B.4) to demonstrate experimental control of the five-spin system and to execute cases of the Deutsch-Jozsa algorithm. For each function ( $f_0$  and  $f_b$ ) the following three sets of experiments were performed (see experimental spectra in Fig. 4). Set 1 (first row of curves from the bottom in Fig. 4): preparation of the linear terms  $I_{kz}$  (with algebraic signs as specified in Eq. (8) and Table II), application of  $U_{90}$  and  $U(f)$ , and detection of spin  $k$  for  $k = 1, \dots, 5$ ; set 2 (second row in Fig. 4): preparation of the bilinear terms  $2I_{kz}I_{\{k+1\}z}$  (with algebraic signs as specified in Eq. (8) and Table II), application of  $U_{90}$  and  $U(f)$ , and detection of spin  $k$  for  $k = 1, \dots, 4$ ; and set 3 (third row in

Fig. 4): preparation of the bilinear terms  $2I_{\{k-1\}z}I_{kz}$  (with

algebraic signs as specified in Eq. (8) and Table II), application of  $U_{90}$  and  $U(f)$ , and detection of spin  $k$  for  $k = 2, \dots, 5$ .

The observed spectra shown in Fig. 4 correspond closely to the theoretical predictions (see Table II). For the constant function  $f_0$ , only the experiments of set 1 yield detectable signals. For the balanced function  $f_b$ , the experiments of set 1 only yield a detectable signal for spin 5, whereas for spins 1–4 detectable signals are only obtained in the experiments of set 2. As expected, only spurious signals are detected for the experiments of set 3. The amplitude of these spurious signals is typically on the order of 4% compared to the full signals. As expected, all the signals of spins 1–4 are positive for the constant function whereas the signal of spin 4 is inverted

by the propagator  $\tilde{U}(f_b)$  corresponding to the balanced function. For  $f_b$  the signal amplitudes reach only between 55% and 70% of the amplitudes found for  $f_0$ . This signal loss can be attributed mainly to relaxation and experimental imperfections during the sequence that implements  $\tilde{U}(f_b)$  (Fig. 3), which has an overall duration of 51.4 ms.

Through combined synthetic, analytic, and spectroscopic work, a five-bit NMR quantum computer was built and shown to implement superposition, quantum interference, and designed unitary transformations. Although obstacles had to be overcome, none were fundamental, and quantum computers with more than five bits will be built. Lots of interesting questions have been raised for future work pertaining to the constraints and opportunities for linking molecular architecture, spectrometer design, and algorithms for NMR quantum computing.

## ACKNOWLEDGMENTS

S.J.G. acknowledges support by the Fonds der Chemischen Industrie and the DFG. R.M. is supported by a stipend of the Fonds der Chemischen Industrie and the Bundesministerium für Bildung und Forschung (BMBF). We thank C. Griesinger, M. Grundl, R. Kerssebaum, B. Luy, R. Mayr-Stein, M. Kettner, M. Reggelin, H. Schwalbe, and A. Tüchelmann for valuable discussions and technical assistance. A.F.F. thanks G. Wagner (Harvard Medical School) for support and encouragement and acknowledges support from National Science Foundation. J.M.M. thanks T. T. Wu (Harvard University) for many critical insights.

## APPENDIX A: SYNTHESIS OF MOLECULE

We purchased 250 mg of  $^{13}\text{C}_2\text{-}^{15}\text{N}$ -glycine from Martek Biosciences Corporation, 6480 Dobbin Road, Columbia, Maryland 21045. The labeled glycine was fully deuterated by treatment with a solution of NaOD in  $\text{D}_2\text{O}$  at  $140^\circ\text{C}$ . The product was dissolved in water for re-protonation while retaining the deuterium atoms in alpha-position. The resulting  $^{13}\text{C}_2\text{-}^{15}\text{N}\text{-}^2\text{D}_2^\alpha$ -glycine was protected in a standard reaction with di-*tert.*-butyl-dicarbonate (BOC-anhydride) as reagent (O. Keller, W. E. Keller, G. van Look and G. Wersin, *Org. Synth.* **63**, 160 (1985)). Finally the carboxylic acid was converted by cyanuric fluoride into the desired acyl fluoride: BOC- $(^{13}\text{C}_2\text{-}^{15}\text{N}\text{-}^2\text{D}_2^\alpha\text{-glycine})\text{-fluoride}$  (L. A. Carpino, E. M. E. Mansour and D. Sadat-Aalaei, *J. Org. Chem.* **56**, 2611 (1991)). The substance dissolved in  $\text{DMSO-D}_6$  at room temperature shows NMR spectra that weaken with a half-life of about a week, indicative of reactions not yet determined. The solution was stable during storage at a temperature of  $-30^\circ\text{C}$ .

## APPENDIX B: NMR PULSE SEQUENCES

For the preparation of the elements of a pseudopure state and the implementation of quantum gates, robust r.f. pulse sequences are desirable. Pulse-sequence parameters with negligible experimental errors are the durations of r.f. pulses and of delays. In addition, the phases of r.f. pulses and of the receiver can be controlled with negligible errors. The most important experimental imperfections are r.f. amplitude errors that result from miscalibrations and from the r.f. field inhomogeneity created by the r.f. coils. In addition to the use of compensating schemes, such as super cycles and composite pulses [10], experimental imperfections can be reduced by designing pulse sequence elements with a minimum number of r.f. pulses. For example, pulses to refocus frequency offset terms in homonuclear spin systems with different chemical shifts can be eliminated by implementing the experiments in the multiple-rotating frame in which the precession frequency of each individual spin is 0 (see section B.1). More generally, pulses can often be eliminated or replaced by phase adjustments with negligible errors (see section B.2). For the available spectrometer, the experimental pulse parameters are summarized in section B.3. The preparation of the elements of the pseudopure state  $\rho_i$  is discussed in section B.4.

### B.1. Implementation of experiments in the multiple rotating frame

For heteronuclear spins with resonance frequencies  $\nu_k$  and  $\nu_l$  in the laboratory frame, the spins are irradiated on-resonance and the observed signals are demodulated by the determined resonance frequencies. If only a single r.f. channel is available for several homonuclear spins, on-resonance irradiation of several homonuclear spins can be achieved using phase-modulation of the r.f. pulses. The reference phase of each pulse applied to spin  $k$  must be adjusted such that it matches the desired phase in the corresponding rotating frame (*vide infra*). In addition, the phases of the detected signals need to be corrected for the relative phases that have been acquired by the respective rotating frames during the course of the experiment. In our case with the two homonuclear spins  $\text{C}^\alpha$  (spin #3) and  $\text{C}'$  (spin #4), the transmitter frequency of the carbon r.f. channel was set to the  $\text{C}^\alpha$  resonance frequency. In order to simplify the combination of different quantum gates, the durations of the pulse sequences for each gate were chosen to be integer multiples of  $\Delta = 1/|\nu_3 - \nu_4| = 81.75 \mu\text{s}$ . Hence, the rotating frames are aligned at the end of each gate.

## B.2. Simplifying pulse sequences

Some quantum gates, such as  $(\text{CNOT})_{kl}$ , require  $z$  rotations of individual spins which can be implemented using composite r.f. pulses [22]. However, these pulses can be avoided if  $z$  rotations (by angle  $\varphi$ ) are implemented by a corresponding negative rotation of the respective rotating frame of reference. In practice, this results in an additional phase shift (by angle  $-\varphi$ ) of all following r.f. pulses that are applied to this spin and of the receiver phase of this spin. Furthermore,  $180_{\vartheta}^{\circ}$  pulses (with arbitrary phase  $\vartheta$ ) are required in some cases to refocus the evolution due to  $J$  couplings. In order to undo the rotation caused by these pulses, additional  $180_{\vartheta}^{\circ}$  or  $180_{-\vartheta}^{\circ}$  pulses are often needed at the beginning or at the end of these quantum gates. An appropriate choice of the position and phase  $\vartheta$  of these pulses often makes it possible to cancel two pulses from adjacent gates (e.g.,  $180_x^{\circ}$  and  $180_{-x}^{\circ}$ ) or to absorb a  $180^{\circ}$  pulse into the phase of an adjacent  $90^{\circ}$  pulse (e.g., a  $180_x^{\circ}$  pulse preceded or followed by a  $90_{-x}^{\circ}$  pulse is equivalent to a single  $90_x^{\circ}$  pulse).

Even if r.f. pulses cannot be completely eliminated, the accumulation of small flip angle errors can be avoided by a proper choice of pulse phases which is common practice in the design of modern NMR multiple pulse sequences [10]. For example, the so-called MLEV-4 expansion [14,15,16]  $180_x^{\circ}180_{-x}^{\circ}180_{-x}^{\circ}180_x^{\circ}$  (used here, e.g., for spin 5 decoupling during spin 3- and spin 4-selective  $90^{\circ}$  pulses) is preferable to  $180_x^{\circ}180_{-x}^{\circ}180_x^{\circ}180_{-x}^{\circ}$  or to  $180_x^{\circ}180_x^{\circ}180_x^{\circ}180_x^{\circ}$ .

## B.3. Experimental pulse parameters

Due to their large frequency separation, selective pulses for spins 1 ( $^1\text{H}$ ), 2 ( $^{15}\text{N}$ ) and 5 ( $^{19}\text{F}$ ) could be implemented by simple square pulses. The durations of  $90^{\circ}$  pulses were  $8.85 \mu\text{s}$ ,  $41 \mu\text{s}$  and  $11.75 \mu\text{s}$ , respectively. For spins 3 ( $^{13}\text{C}^{\alpha}$ ) and 4 ( $^{13}\text{C}'$ ) the following shaped pulses with minimal durations and optimal selectivity were chosen based on numerical simulations and experimental optimizations:  $90^{\circ}$  pulses were implemented as e-SNOB pulses [23], not for the usual  $270^{\circ}$ , but for a  $90^{\circ}$

rotation with a duration of  $224 \mu\text{s}$ ; selective  $180^{\circ}$  pulses were implemented as Gaussian pulses [24] with a duration of  $250 \mu\text{s}$  and a truncation level of 20%. The application of these shaped e-SNOB and Gaussian pulses on  $\text{C}^{\alpha}$  has a nonresonant effect [25] on  $\text{C}'$  which corresponds to experimentally determined  $z$  rotations of  $\varphi_e = -4^{\circ}$  and  $\varphi_g = -18^{\circ}$ , respectively. Conversely, a shaped e-SNOB pulse applied to  $\text{C}'$  leads to a  $z$  rotation of  $-\varphi_e$  for  $\text{C}^{\alpha}$ . In all experiments these phase shifts were taken into account by adjusting the phases of the following pulse and the receiver phases (see Fig. 3). (Note that the phases of the two selective Gaussian  $180^{\circ}$  pulses applied to spin 3 in the period  $\tau_{45}$  is not corrected because their absolute

phases are arbitrary, c.f. Appendix B.2.) During the spin 3- or spin 4-selective  $180^{\circ}$  pulses, the evolution due to the strong  $J_{35}$  and  $J_{45}$  couplings is automatically refocused. As this is not the case for spin 3- or spin 4-selective  $90^{\circ}$  pulses, spin 5 was actively decoupled during these pulses (see Fig. 3).

As commercial high-resolution NMR spectrometers are commonly not equipped with multiple receivers, it was not possible to simultaneously detect the signals of different spin species. Moreover, the application of any given pulse sequence required four different pulse programs because the routing of the r.f. channels (for the creation of  $^1\text{H}$ ,  $^{15}\text{N}$ ,  $^{13}\text{C}$ ,  $^{19}\text{F}$  and  $^2\text{D}$  pulses) depends on the detected spin species ( $^1\text{H}$ ,  $^{15}\text{N}$ ,  $^{13}\text{C}$  or  $^{19}\text{F}$ ). Due to this technical limitation, each spin species had to be detected in a separate experiment for every term of the initial density operator  $\rho_i$ . However, this made it possible to use standard heteronuclear decoupling techniques to simplify the detected signals and to significantly increase the signal-to-noise ratio of the experiments.

During spin 1 detection, spins 2 and 3 were decoupled with an r.f. amplitude  $\nu_{rf} = \gamma B_{rf}/(2\pi)$  of 0.6 kHz and 0.4 kHz, respectively. During spin 2 detection, spins 1 and 3 were decoupled with an r.f. amplitude of 2.3 kHz and 0.4 kHz, respectively. During spin 3 detection, spins 1, 2 and 5 were decoupled with an r.f. amplitude of 2.3 kHz, 0.6 kHz and 2.0 kHz, respectively, and during spin 4 detection, spin 5 was decoupled with an r.f. amplitude of 2.0 kHz. In all these cases, the WALTZ-16 decoupling sequence [14,15,16] was used. In principle, also the  $J_{34}$  coupling could be effectively eliminated during detection of spin 3 or spin 4 using time-shared decoupling. However, this was not possible with our experimental setup because more than five separate r.f. channels would have been required. From the resulting doublets (with splitting  $J_{34}$ ) an apparent singlet was created by merging the two doublet components [26]. During spin 5 detection, spins 3 and 4 were simultaneously decoupled using a double-selective G3-MLEV sequence [14,15,16] with an r.f. amplitude of 6 kHz. In addition, during all experiments deuterium decoupling was applied using a WALTZ-16 sequence with  $\nu_{rf} = 0.5$  kHz. In order to approximate a constant sample temperature of about  $27^{\circ}\text{C}$  in spite of the additional sample heating effected by the decoupling sequences, 16 dummy scans were used prior to signal acquisition of spins 1 and 5, whereas 4 dummy scans were used prior to signal acquisition of spins 2, 3, and 4. Nevertheless, the linewidths of the experimental signals shown in Fig. 4 were slightly increased by residual sample heating effects and imperfections of the decoupling sequences.

#### B.4. Pulse sequences for the preparation of the terms of $\rho_i$ and $\rho_0$

In order to improve the sensitivity of the experiments and to filter out signals from impurities in the sample, individual Cartesian product operator terms of  $\rho_i$  were created using sequential INEPT transfer steps [21] starting from  $^1\text{H}$  magnetization, corresponding to the operator  $I_{1z}$ . The term  $I_{1z}$  was prepared from the thermal equilibrium density operator by applying spin 2, 3, 4, and 5 selective  $90^\circ$  pulses followed by a pulsed field gradient of the static magnetic field. An X-filter element [27] was used to select  $^1\text{H}$  spins that are coupled to  $^{15}\text{N}$ . For the preparation of other terms of  $\rho_i$  (starting from  $I_{1z}$ ), the phase  $\phi_a$  of the first  $90^\circ$  pulse applied to spin 1 was subject to a two-step phase cycle. In addition, the phase  $\phi_b$  of the  $90^\circ$  pulses for the implementation of  $U_0$  (see Eq. (4)) was also subject to an independent phase cycle. Overall, this resulted in a four-step phase cycle with the pulse phases  $\phi_a = \{0^\circ, 180^\circ, 0^\circ, 180^\circ\}$ ,  $\phi_b = \{90^\circ, 90^\circ, 270^\circ, 270^\circ\}$  and the relative receiver phases  $\phi_{\text{rec}} = \{0^\circ, 180^\circ, 0^\circ, 180^\circ\}$ .

#### APPENDIX C: DENSITY OPERATOR TERMS

For all 31 Cartesian product operator terms in  $\rho_i$  (Eq. (8)), the corresponding terms in  $\rho_0$  and  $\tilde{\rho}_b$  are summarized in Table III. The transformation  $\rho_0 \xrightarrow{\tilde{U}(f_b)} \tilde{\rho}_b$  of the unitary operator corresponding to the balanced function  $f_b$  is composed of four consecutive unitary transformations corresponding to (CNOT) $_{kl}$  quantum gates:

$$\rho_0 \xrightarrow{\text{(CNOT)}_{12}} \rho' \xrightarrow{\text{(CNOT)}_{23}} \rho'' \xrightarrow{\text{(CNOT)}_{34}} \rho''' \xrightarrow{\text{(CNOT)}_{45}} \tilde{\rho}_b.$$

The transformations of the individual (CNOT) $_{kl}$  gates can be derived using the following rules [2]:

$$\begin{aligned} I_{kx} &\xrightarrow{\text{(CNOT)}_{kl}} 2I_{kx}I_{lx}, \\ 2I_{kx}I_{lx} &\xrightarrow{\text{(CNOT)}_{kl}} I_{kx}, \\ I_{lx} &\xrightarrow{\text{(CNOT)}_{kl}} I_{lx}. \end{aligned}$$

The terms of the intermediate operators  $\rho'$ ,  $\rho''$  and  $\rho'''$  are also given in Table III for completeness.

- 
- [1] C. Monroe, D. M. Meekhof, B. E. King, W. M. Itano, and D. J. Wineland, Phys. Rev. Lett. **75**, 4714 (1995).  
[2] N. Linden, H. Barjat, and R. Freeman, Chem. Phys. Lett. **296**, 61 (1998).  
[3] Z. L. Mádi, R. Brüschweiler, and R. R. Ernst, J. Chem. Phys. **109**, 10603 (1998).  
[4] D. Deutsch, and R. Jozsa, Proc. Roy. Soc. London A **439**, 553 (1992).

- [5] C. H. Bennett, IBM J. Res. Devel., November, 525 (1973).  
[6] J. M. Myers, Phys. Rev. Lett. **78**, 1823 (1997).  
[7] D. G. Cory, A. F. Fahmy, and T. F. Havel, "Nuclear magnetic resonance spectroscopy: An experimentally accessible paradigm for quantum computing," in *Proc. of the 4th Workshop on Physics and Computation* (New England Complex Systems Institute, Boston, MA, 1996), pp. 87–91.  
[8] D. G. Cory, A. F. Fahmy, and T. F. Havel, Proc. Natl. Acad. Sci. USA **94**, 1634 (1997).  
[9] N. A. Gershenfeld, and I. L. Chuang, Science **275**, 350 (1997).  
[10] R. R. Ernst, G. Bodenhausen, and A. Wokaun, *Principles of Nuclear Magnetic Resonance in One and Two Dimensions* (Oxford University Press, Oxford, 1987).  
[11] R. Cleve, A. Ekert, C. Macchiavello, and M. Mosca, Proc. Roy. Soc. London A **454**, 339 (1998).  
[12] J. A. Jones, and M. Mosca, J. Chem. Phys. **109**, 1648 (1998).  
[13] D. Collins, K. W. Kim, and W. C. Holton, Phys. Rev. A **58**, R1633 (1998).  
[14] M. H. Levitt, R. Freeman, and T. Frenkiel, "Broadband decoupling in high-resolution nuclear magnetic resonance spectroscopy" in *Advances in Magnetic Resonance*, J. S. Waugh, Ed. (Academic Press, New York, 1983), vol. 11, pp. 47–110.  
[15] A. J. Shaka, J. Keeler, T. Frenkiel, and R. Freeman, J. Magn. Reson. **52**, 335 (1983).  
[16] U. Eggenberger, P. Schmidt, M. Sattler, S. J. Glaser, and C. Griesinger, J. Magn. Reson. **100**, 604 (1992).  
[17] U. Haeberlen, and J. S. Waugh, Phys. Rev. **175**, 453 (1968).  
[18] S. J. Glaser, and J. J. Quant, "Homonuclear and heteronuclear Hartmann-Hahn transfer in isotropic liquids," in *Advances in Magnetic and Optical Resonance*, W. S. Warren, Ed. (Academic Press, New York, 1996), vol. 19, pp. 59–252.  
[19] S. J. Glaser, T. Schulte-Herbrüggen, M. Sieveking, O. Schedletsky, N. C. Nielsen, O. W. Sørensen, and C. Griesinger, Science **280**, 421 (1998).  
[20] E. Knill, I. L. Chuang, and R. Laflamme, Phys. Rev. A **57**, 3348 (1998).  
[21] G. A. Morris, and R. Freeman, J. Am. Chem. Soc. **101**, 760 (1979).  
[22] R. Freeman, T. A. Frenkiel, and M. Levitt, J. Magn. Reson. **44**, 409 (1981).  
[23] Ě. Kupče, J. Boyd, and I. D. Campbell, J. Magn. Reson. B **106**, 300 (1995).  
[24] C. Bauer, R. Freeman, T. Frenkiel, J. Keeler, and A. J. Shaka, J. Magn. Reson. **58**, 442 (1984).  
[25] M. A. McCoy, and L. Müller, J. Magn. Reson. **99**, 18 (1992).  
[26] M. Sattler, J. Schleucher, O. Schedletsky, S. J. Glaser, C. Griesinger, N. C. Nielsen, and O. W. Sørensen, J. Magn. Reson. A **119**, 171 (1996).  
[27] E. Wörgötter, G. Wagner, and K. Wüthrich, J. Am. Chem. Soc. **108**, 6162 (1986).



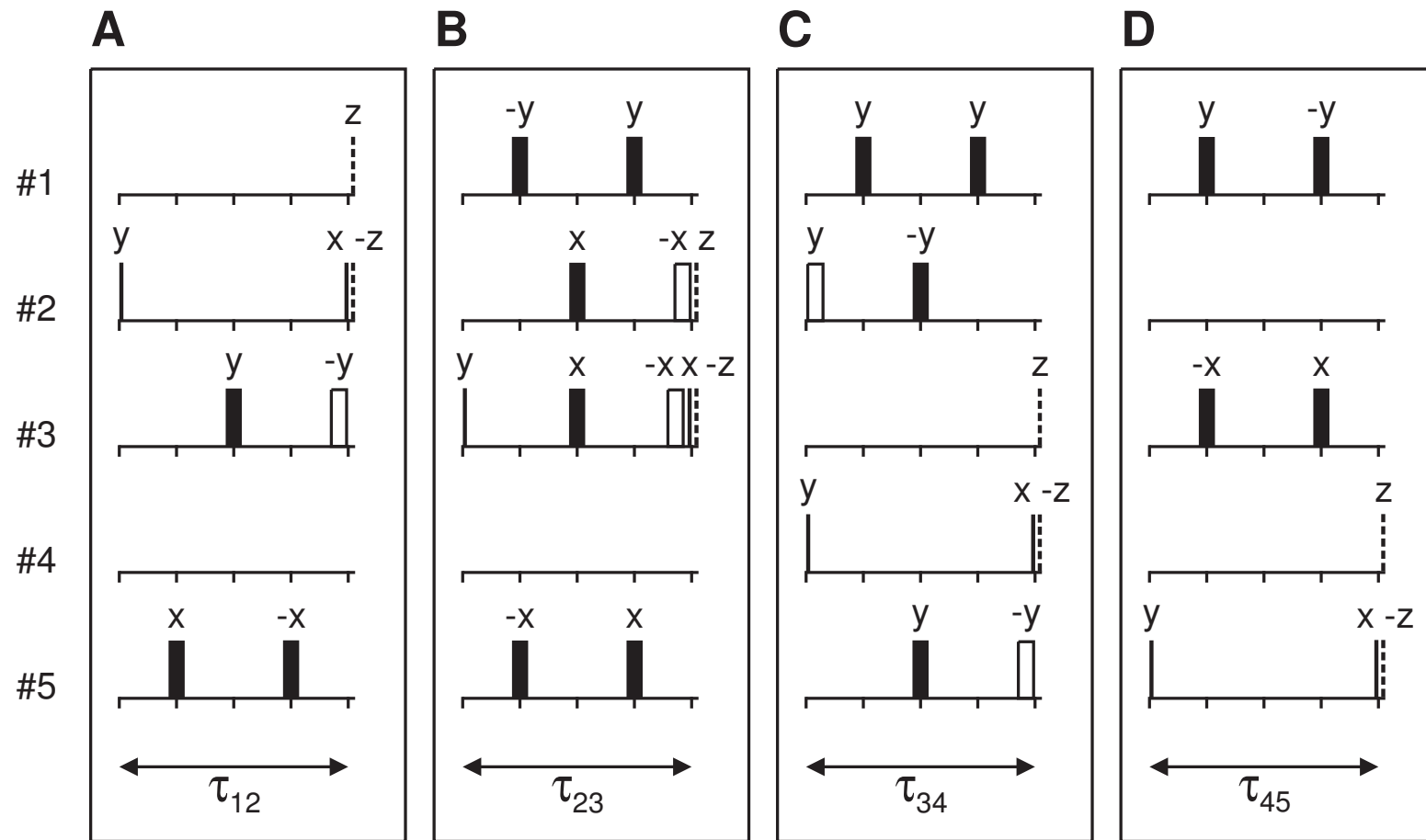


Figure 2

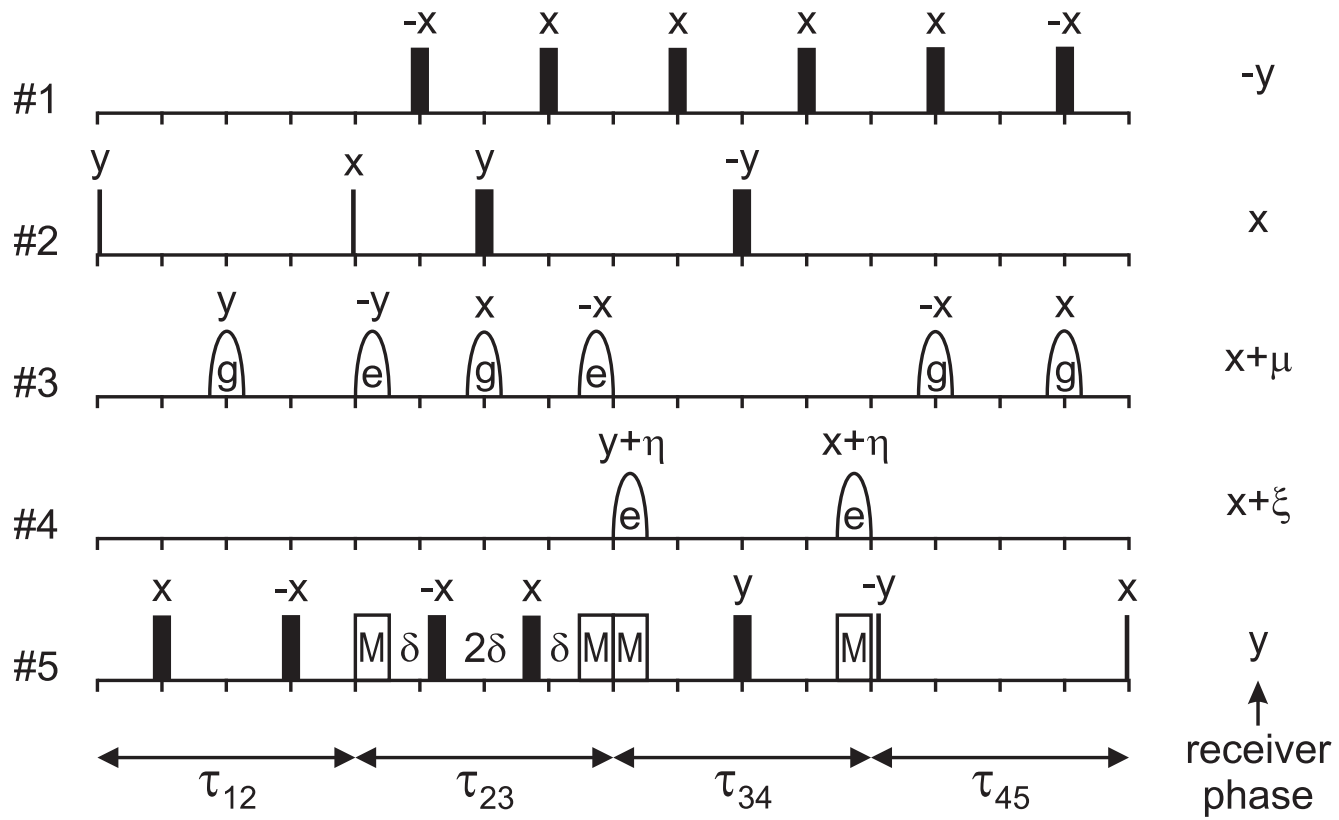


Figure 3

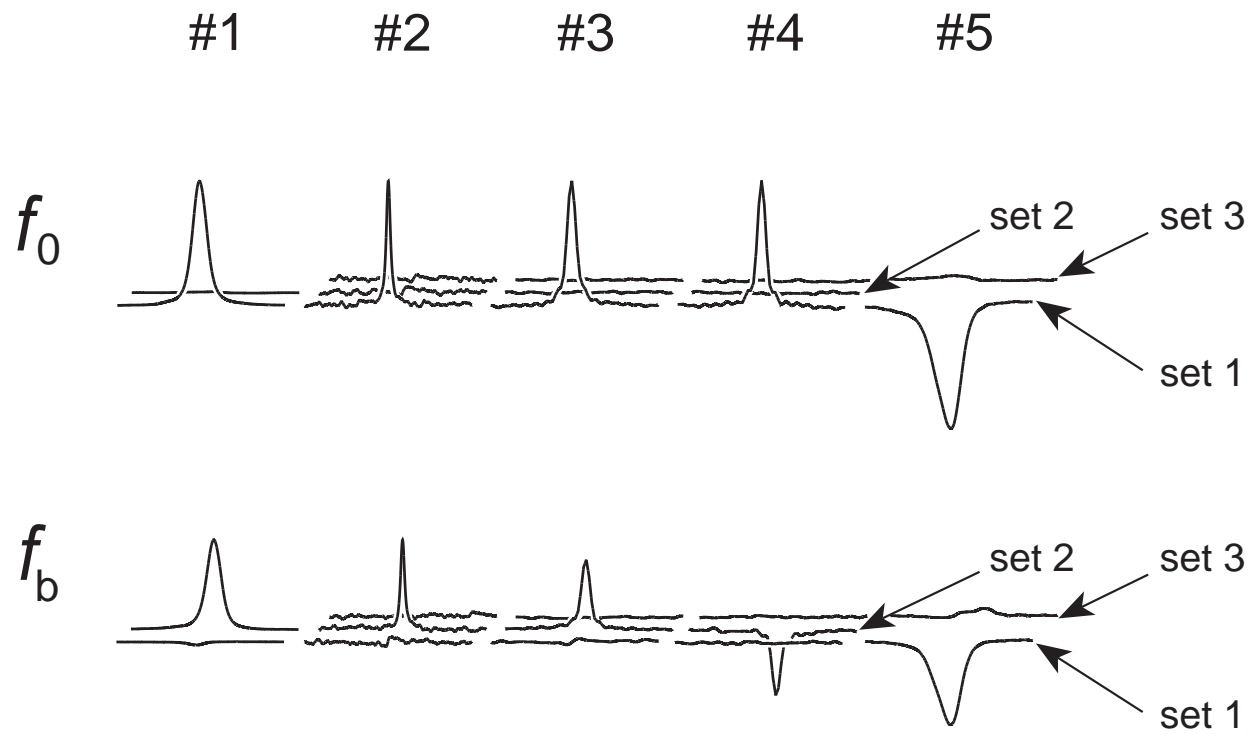


Figure 4

TABLE III. Terms of operators.

$\rho_i$	$\rho_0$	$\rho'$	$\rho''$	$\rho'''$	$\tilde{\rho}_b$
$I_{1z}$	<u><math>I_{1x}</math></u>	$2I_{1x}I_{2x}$	$4I_{1x}I_{2x}I_{3x}$	$8I_{1x}I_{2x}I_{3x}I_{4x}$	$16I_{1x}I_{2x}I_{3x}I_{4x}I_{5x}$
$I_{2z}$	<u><math>I_{2x}</math></u>	$I_{2x}$	$2I_{2x}I_{3x}$	$4I_{2x}I_{3x}I_{4x}$	$8I_{2x}I_{3x}I_{4x}I_{5x}$
$I_{3z}$	<u><math>I_{3x}</math></u>	$I_{3x}$	$I_{3x}$	$2I_{3x}I_{4x}$	$4I_{3x}I_{4x}I_{5x}$
$I_{4z}$	<u><math>I_{4x}</math></u>	$I_{4x}$	$I_{4x}$	$I_{4x}$	$2I_{4x}I_{5x}$
$-I_{5z}$	<u><math>-I_{5x}</math></u>	$-I_{5x}$	$-I_{5x}$	$-I_{5x}$	<u><math>-I_{5x}</math></u>
$2I_{1z}I_{2z}$	$2I_{1x}I_{2x}$	$I_{1x}$	$I_{1x}$	$I_{1x}$	<u><math>I_{1x}</math></u>
$2I_{1z}I_{3z}$	$2I_{1x}I_{3x}$	$4I_{1x}I_{2x}I_{3x}$	$2I_{1x}I_{2x}$	$2I_{1x}I_{2x}$	<u><math>2I_{1x}I_{2x}</math></u>
$2I_{1z}I_{4z}$	$2I_{1x}I_{4x}$	$4I_{1x}I_{2x}I_{4x}$	$8I_{1x}I_{2x}I_{3x}I_{4x}$	$4I_{1x}I_{2x}I_{3x}$	$4I_{1x}I_{2x}I_{3x}$
$-2I_{1z}I_{5z}$	$-2I_{1x}I_{5x}$	$-4I_{1x}I_{2x}I_{5x}$	$-8I_{1x}I_{2x}I_{3x}I_{5x}$	$-16I_{1x}I_{2x}I_{3x}I_{4x}I_{5x}$	$-8I_{1x}I_{2x}I_{3x}I_{4x}$
$2I_{2z}I_{3z}$	$2I_{2x}I_{3x}$	$2I_{2x}I_{3x}$	$I_{2x}$	$I_{2x}$	<u><math>I_{2x}</math></u>
$2I_{2z}I_{4z}$	$2I_{2x}I_{4x}$	$2I_{2x}I_{4x}$	$4I_{2x}I_{3x}I_{4x}$	$2I_{2x}I_{3x}$	<u><math>2I_{2x}I_{3x}</math></u>
$-2I_{2z}I_{5z}$	$-2I_{2x}I_{5x}$	$-2I_{2x}I_{5x}$	$-4I_{2x}I_{3x}I_{5x}$	$-8I_{2x}I_{3x}I_{4x}I_{5x}$	$-4I_{2x}I_{3x}I_{4x}$
$2I_{3z}I_{4z}$	$2I_{3x}I_{4x}$	$2I_{3x}I_{4x}$	$2I_{3x}I_{4x}$	$I_{3x}$	<u><math>I_{3x}</math></u>
$-2I_{3z}I_{5z}$	$-2I_{3x}I_{5x}$	$-2I_{3x}I_{5x}$	$-2I_{3x}I_{5x}$	$-4I_{3x}I_{4x}I_{5x}$	$-2I_{3x}I_{4x}$
$-2I_{4z}I_{5z}$	$-2I_{4x}I_{5x}$	$-2I_{4x}I_{5x}$	$-2I_{4x}I_{5x}$	$-2I_{4x}I_{5x}$	<u><math>-I_{4x}</math></u>
$4I_{1z}I_{2z}I_{3z}$	$4I_{1x}I_{2x}I_{3x}$	$2I_{1x}I_{3x}$	$2I_{1x}I_{3x}$	$4I_{1x}I_{3x}I_{4x}$	$8I_{1x}I_{3x}I_{4x}I_{5x}$
$4I_{1z}I_{2z}I_{4z}$	$4I_{1x}I_{2x}I_{4x}$	$2I_{1x}I_{4x}$	$2I_{1x}I_{4x}$	$2I_{1x}I_{4x}$	$4I_{1x}I_{4x}I_{5x}$
$-4I_{1z}I_{2z}I_{5z}$	$-4I_{1x}I_{2x}I_{5x}$	$-2I_{1x}I_{5x}$	$-2I_{1x}I_{5x}$	$-2I_{1x}I_{5x}$	$-2I_{1x}I_{5x}$
$4I_{1z}I_{3z}I_{4z}$	$4I_{1x}I_{3x}I_{4x}$	$8I_{1x}I_{2x}I_{3x}I_{4x}$	$4I_{1x}I_{2x}I_{4x}$	$4I_{1x}I_{2x}I_{4x}$	$8I_{1x}I_{2x}I_{4x}I_{5x}$
$-4I_{1z}I_{3z}I_{5z}$	$-4I_{1x}I_{3x}I_{5x}$	$-8I_{1x}I_{2x}I_{3x}I_{5x}$	$-4I_{1x}I_{2x}I_{5x}$	$-4I_{1x}I_{2x}I_{5x}$	$-4I_{1x}I_{2x}I_{5x}$
$-4I_{1z}I_{4z}I_{5z}$	$-4I_{1x}I_{4x}I_{5x}$	$-8I_{1x}I_{2x}I_{4x}I_{5x}$	$-16I_{1x}I_{2x}I_{3x}I_{4x}I_{5x}$	$-8I_{1x}I_{2x}I_{3x}I_{5x}$	$-8I_{1x}I_{2x}I_{3x}I_{5x}$
$4I_{2z}I_{3z}I_{4z}$	$4I_{2x}I_{3x}I_{4x}$	$4I_{2x}I_{3x}I_{4x}$	$2I_{2x}I_{4x}$	$2I_{2x}I_{4x}$	$4I_{2x}I_{4x}I_{5x}$
$-4I_{2z}I_{3z}I_{5z}$	$-4I_{2x}I_{3x}I_{5x}$	$-4I_{2x}I_{3x}I_{5x}$	$-2I_{2x}I_{5x}$	$-2I_{2x}I_{5x}$	$-2I_{2x}I_{5x}$
$-4I_{2z}I_{4z}I_{5z}$	$-4I_{2x}I_{4x}I_{5x}$	$-4I_{2x}I_{4x}I_{5x}$	$-8I_{2x}I_{3x}I_{4x}I_{5x}$	$-4I_{2x}I_{3x}I_{5x}$	$-4I_{2x}I_{3x}I_{5x}$
$-4I_{3z}I_{4z}I_{5z}$	$-4I_{3x}I_{4x}I_{5x}$	$-4I_{3x}I_{4x}I_{5x}$	$-4I_{3x}I_{4x}I_{5x}$	$-2I_{3x}I_{5x}$	$-2I_{3x}I_{5x}$
$8I_{1z}I_{2z}I_{3z}I_{4z}$	$8I_{1x}I_{2x}I_{3x}I_{4x}$	$4I_{1x}I_{3x}I_{4x}$	$4I_{1x}I_{3x}I_{4x}$	$2I_{1x}I_{3x}$	$2I_{1x}I_{3x}$
$-8I_{1z}I_{2z}I_{3z}I_{5z}$	$-8I_{1x}I_{2x}I_{3x}I_{5x}$	$-4I_{1x}I_{3x}I_{5x}$	$-4I_{1x}I_{3x}I_{5x}$	$-8I_{1x}I_{3x}I_{4x}I_{5x}$	$-4I_{1x}I_{3x}I_{4x}$
$-8I_{1z}I_{2z}I_{4z}I_{5z}$	$-8I_{1x}I_{2x}I_{4x}I_{5x}$	$-4I_{1x}I_{4x}I_{5x}$	$-4I_{1x}I_{4x}I_{5x}$	$-4I_{1x}I_{4x}I_{4x}$	$-2I_{1x}I_{4x}$
$-8I_{1z}I_{3z}I_{4z}I_{5z}$	$-8I_{1x}I_{3x}I_{4x}I_{5x}$	$-16I_{1x}I_{2x}I_{3x}I_{4x}I_{5x}$	$-8I_{1x}I_{2x}I_{4x}I_{5x}$	$-8I_{1x}I_{2x}I_{4x}I_{5x}$	$-4I_{1x}I_{2x}I_{4x}$
$-8I_{2z}I_{3z}I_{4z}I_{5z}$	$-8I_{2x}I_{3x}I_{4x}I_{5x}$	$-8I_{2x}I_{3x}I_{4x}I_{5x}$	$-4I_{2x}I_{4x}I_{5x}$	$-4I_{2x}I_{4x}I_{5x}$	$-2I_{2x}I_{4x}$
$-16I_{1z}I_{2z}I_{3z}I_{4z}I_{5z}$	$-16I_{1x}I_{2x}I_{3x}I_{4x}I_{5x}$	$-8I_{1x}I_{3x}I_{4x}I_{5x}$	$-8I_{1x}I_{3x}I_{4x}I_{5x}$	$-4I_{1x}I_{3x}I_{5x}$	$-4I_{1x}I_{3x}I_{5x}$

 Note: detectable terms of  $\rho_0$  and  $\tilde{\rho}_b$  are underlined.